Journal of Glaciology, Vol. 34, No. 117, 1988

INSTRUMENTS AND METHODS

MICROCOMPUTER-BASED IMAGE-PROCESSING SYSTEM

By DONALD K. PEROVICH

(U.S. Army Cold Regions Research and Engineering Laboratory,

Hanover, New Hampshire 03755-1290, U.S.A.)

and AKIRA HIRAI

(Department of Engineering Sciences, Harvard College, Cambridge,

Massachusetts 02138, U.S.A.)

ABSTRACT. Inexpensive add-on boards are currently available that enable personal computers to be used as digital image-processing systems. The capabilities of one such system are illustrated by two specific cases examining the surface characterization of a sea-ice cover and the statistical description of sea-ice structure. The unit discussed digitizes video input into a 512 × 512 array of pixels, assigning each a gray shade from 0 to 255. A key feature of the system is that the primitive commands of the board can be accessed through higher-level programming languages. This allows users to customize easily the system for their own needs.

INTRODUCTION

There is a wide range of glaciological problems for which computer-based digital image-processing techniques are particularly well suited. Applications range from the interpretation of remote-sensing data (Carsey and Zwally, 1986) to studies of snow sterology. In the past, such activities have been the province of large, dedicated systems, with costs beyond the resources of many researchers. Those with more modest means and needs were forced to reply on labor-intensive techniques such as planimetry, hand digitization, and counting squares. Recently, this limitation has been overcome with the advent of inexpensive image-processing boards designed for use with personal computers.

We have been involved with both the software development and the use of a system that consists of an image board and an IBM-compatible personal computer (Greeley and others, 1987). Our uses have included surface characterization using aerial photography and quantitative analysis of the micro-structure of sea ice. While this system may not have the speed or the storage capacity of more elaborate units that are orders of magnitude more expensive, we have found it to be very powerful and robust. It is the purpose of this paper to outline the general capabilities of this system and to provide examples of its uses.

THE SYSTEM

Several companies make image-processing boards for use with microcomputers. Our particular system consists of a Matrox Pip-1024 image-processing board installed in a Compaq 386 microcomputer. The Pip-1024 is a plug-in board costing approximately $2000 that enables an IBM-compatible microcomputer to perform frame-grabbing operations on an external source video signal (Matrox Electronics Systems Limited, 1986). The source can be either a video camera or a video-cassette recorder. The board has one megabyte of eight-bit memory that typically is partitioned into quadrants. When a video frame is grabbed, it is digitized into a 512 × 512 array of pixels with each pixel assigned a gray shade from 0 (dark) to 255 (bright). The system discussed here inputs images only in black and white, though a three-color version is available for roughly twice the cost. There are also eight independently selectable look-up tables, each allowing for the display of 256 colors chosen from a palette of over 16 million.

Accompanying the hardware is a software library of primitive commands designed to eliminate the need to interface directly with the image board. These commands enable a user to perform a wide range of image-processing tasks including frame input and output, look-up table manipulation, screen graphics, and image convolution. In practice, entering these commands directly from the keyboard is both time consuming and awkward. The most powerful feature of the bundled software is that the library can be accessed by either Fortran or C programs. Linking the routines with a higher-level language greatly increases ease of use, speed, and flexibility.

We capitalized on this feature by writing a user-friendly interface to the Matrox hardware and software. Because of significantly faster execution times, the interface was written in C rather than Fortran The end result is a customized, user-friendly, menu-driven software package, where it is not necessary to invoke a long list of arcane commands. Using the menus, it is possible by using only a few key strokes to grab a frame, store a frame on disk, calculate a gray-scale histogram, false-color an image, execute an edge detection algorithm, or perform a number of other tasks.

The host microcomputer was a Compaq 386 (IBM compatible) with an 80386 processor runing at 16 MHz with a 40 megabyte hard disk. Although a hard disk is not required, it greatly increases the utility of the system. We found the system speed to be more than adequate. Frame grabbing is in real time at the standard rate of 1/30 s. Retrieving or storing an image from a disk takes 2 s using a hard disk and 17 s using a floppy disk. Histograms are calculated in 2 s, while convolving an image with a 3 × 3 kernel takes 13 s. False-color manipulations and switching between the eight available look-up tables or the four image quadrants are essentially instantaneous. Execution times are roughly proportional to the microprocessor clock speed. For example, on a system running at 8 MHz times would be approximately doubled.

APPLICATIONS

To illustrate some of the capabilities of this system, let us examine two specific applications: (1) large-scale characterization of sea-ice cover, and (2) small-scale statistical description of ice structure.

Large-scale surface characterization

When characterizing a sea-ice cover, the simplest question we can ask is what fraction of the area is covered by ice and what fraction by water. Ice concentration is important both as an input parameter and as a diagnostic of large-scale ice/ocean models (Tucker and Hibler, 1987). In winter the area of open water is important in ice-production studies (Maykut, 1982) and in summer for ice-cover decay (Langleben, 1972; Perovich, unpublished).

Figure 1 is the digitized image of an aerial photograph taken on 25 June during the 1984 Marginal Ice Zone Experiment. The photograph was taken 6 km from the ice edge (Hall, 1984) at an altitude of 250 m. In this case, the source image was a photographic print, but a photographic negative or a video tape would have served equally well.

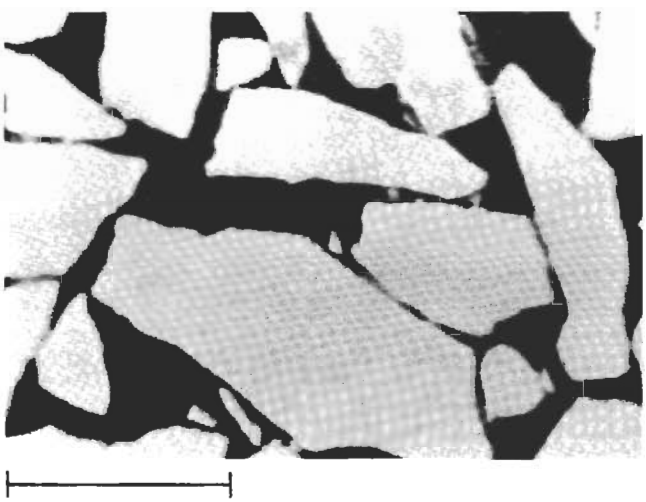

Fig. 1. Digitized version of an aerial photograph taken on 25 June during the 1984 Marginal Ice Zone Experiment from an altitude of 800 m. The original photograph was digitized into a 512 × 512 array of pixels. The horizontal line is 100 m. (Original photograph by R.T. Hall.)

The objective of the analysis was to determine the relative areas of ice and open water. The histogram (Fig. 2) of this image shows a sharp peak at dark gray shades and a broader peak at bright values, connected by a broad shallow valley. Examining the image and the histograms, it was clear that the dark peak was open water and the light peak was ice. Two techniques were used to ascertain what the broad valley was and to determine the exact gray shade cut-off between ice and open water. A cursor was moved about the image and used to interrogate the gray-shade value for pixels of known surface type. After obtaining an approximate idea of the appropriate gray-shade values for different surface types, a false-color rendition of the image was created. Different false-color schemes were tested and the false-color ranges adjusted interactively until a suitable map was produced. In Figure 3 the image is divided into open water (black), flooded ice (gray), and bare or snow-covered ice (white). Open water covered 23% of the area (gray shades 0–31), under-water shelves and flooded ice covered 5% (32–77), and the remaining 72% (77–160) was bare ice or snow-covered ice.

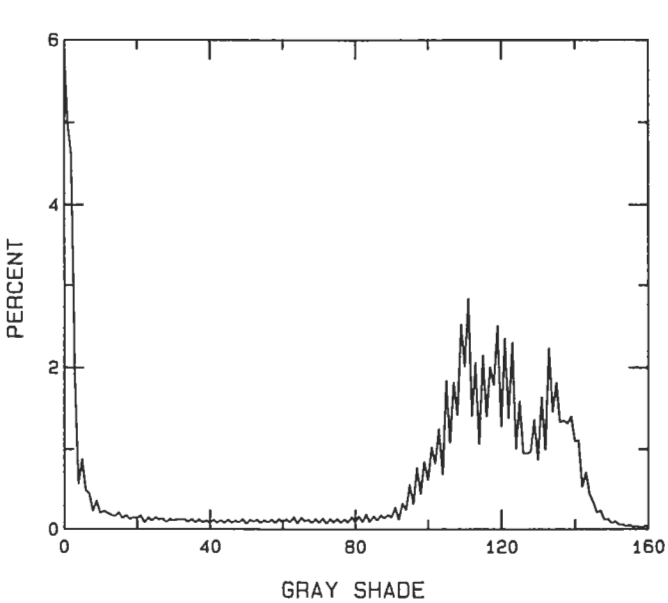

Fig. 2. Gray-shade histogram of the image in Figure 1. Low values of gray shade are dark and high values are bright. The sharp peak near zero is open water and the broad peak from 100 to 160 is bare or snow-covered ice.

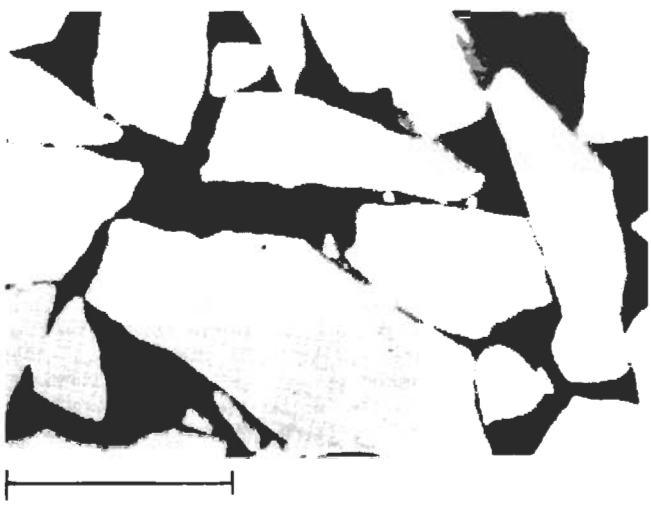

Fig. 3. False-color representation of Figure 1. The spectrum of gray shades has been divided into three types: black for open water, gray for flooded ice, and white for bare or snow-covered ice.

The 32–77 region also includes some pixels on floe edges that contained a combination of ice and water, and introduces what is essentially a resolution error. In a simple image, such as Figure 1, relative areas are accurate to better than ½%. We have also extended this sort of analysis to include areas covered by other ice types such as melt ponds and gray ice. The entire analysis of an image from capture to the final determination of relative areas typically took 5 min.

There are many applications, such as assessing the role of lateral melting in ice-cover decay (Maykut and Perovich, 1987), where the floe perimeter is important. In Figure 4 the image in Figure 3 (with gray set to black) is convolved with the 3 × 3 edge-detection kernel

$$\begin{matrix} 0 & -1 & 0 \\ -1 & 4 & -1 \\ 0 & -1 & 0 \end{matrix}$$

(Pavlidis, 1982), graphically highlighting the floe perimeter.

Statistical description of sea-ice micro-structure

In microwave-modeling efforts, researchers have successfully characterized snow and ice as random media statistically described by a covariance function (Vallese and Kong, 1981). Random media models are also being applied to passive and active microwave studies of sea ice. We have incorporated a feature into our image-processing software to calculate the normalized covariance function (NCF) of a sub-image compared to a main image. This attribute is a good example of the power inherent in accessing the primitive image-processing commands through a higher-level language. It was straightforward to add a compute NCF option to our software menu by incorporating pixel read and write commands into a statistical sub-routine programmed in C.

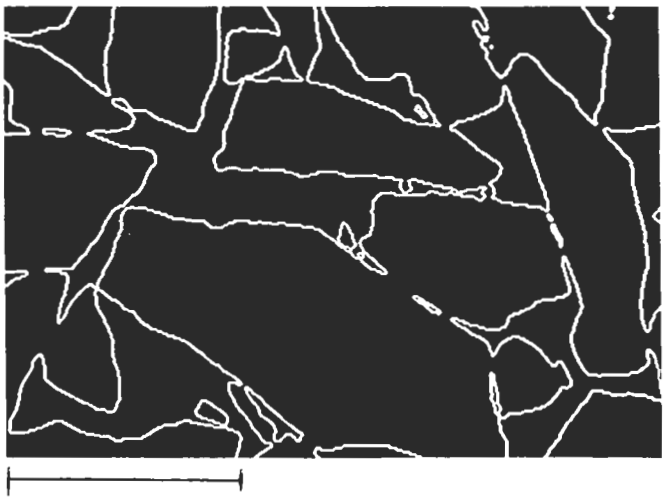

Fig. 4. Image of Figure 1 highlighting the floe perimeter. This image was generated by setting the gray in Figure 3 to white, then convolving with a 3 × 3 edge-detection kernel.

Consider an $m' \times n'$ pixel image with an $m \times n$ pixel sub-image. The NCF of the sub-image (F) with the image (G) at point x,y is defined as

$$\mathrm{NCF} = \frac{1}{\sigma_F \sigma_G} \sum_{i=1}^{m} \sum_{j=1}^{n} F(i,j)G(x+i,\ y+j) - \mu_F \mu_G$$

where μ_F, σ_F, μ_G, σ_G are respectively the mean and standard deviation of the sub-image F and the main image G (Papoulis, 1965). The NCF ranges from −1 to 1, with a value of 1 meaning perfect correspondence between image and sub-image, zero meaning no relationship between image and sub-image, and −1 resulting from a comparison of a sub-image with its complement.

Figure 5 is the digitized image of a microphotograph of first-year sea ice grown in an outdoor tank at the United States Army Cold Regions Research and Engineering Laboratory (Arcone and others, 1986). The ice sample was a horizontal thin section taken from the bottom of a 120 mm thick sheet of ice. The ice was photographed at an air temperature of −10°C.

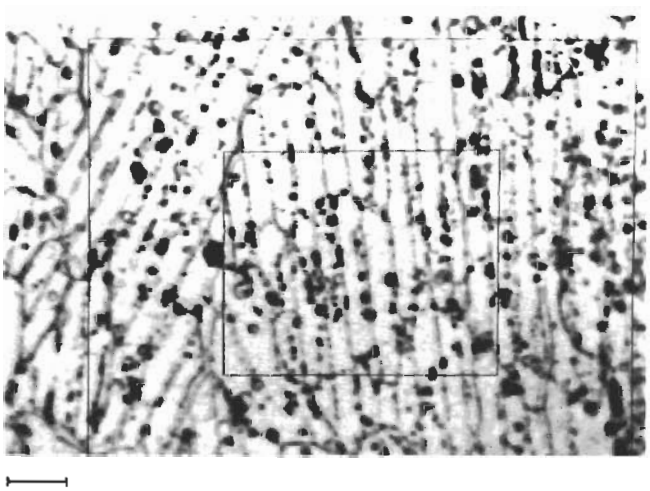

Fig. 5. Digitized version of a microphotograph of a horizontal thin section of sea ice. The two black squares define the image and the sub-image. The sub-image is a 200 × 200 array centered in the 400 × 400 main image. The horizontal line is 1 mm long. (Original photograph by A.J. Gow.)

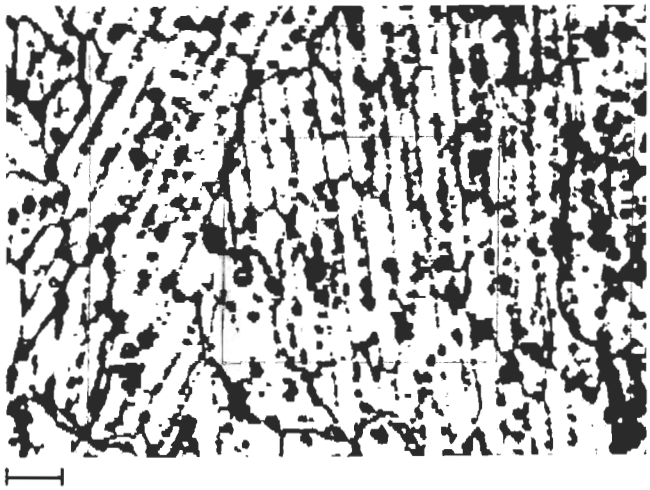

Fig. 6. Two-component representation of Figure 5. In this image the brine is black and the ice is white. The horizontal line is 1 mm long.

Using the methods described in the previous example, the image was divided into its two components of ice and brine. The result is Figure 6, with the white representing ice and the black brine. Since it is a two-component mixture, the NCF does not depend on the absolute values assigned to ice and brine (Stogryn, 1984). No attempt was made to discriminate between vapor and brine inclusions. We then selected a 400 × 400 main image and a 200 × 200 sub-image, as defined by the black borders in Figure 5, and calculated the NCF at every other grid point (10 201 total values). Determining the NCF is a very computationally intensive process that took approximately 16 h to execute in this case.

As Figure 7 illustrates, the NCF for sea ice measured in the XY-plane is asymmetric, dropping off much faster in the X direction that the Y direction. Thus, the distance to decrease to $1/e$, i.e. the correlation length, is represented by an ellipsoid. We suspect that the correlation length also varies in the XZ- and YZ-planes. Figure 8 shows cross-sections taken through the middle of Figure 7 in the X- and the Y-directions. The correlation length is approximately 0.5 mm in the Y-direction and 1.5 mm in the X-direction. These dimensions correspond roughly to the physical dimensons of the small ice platelets.

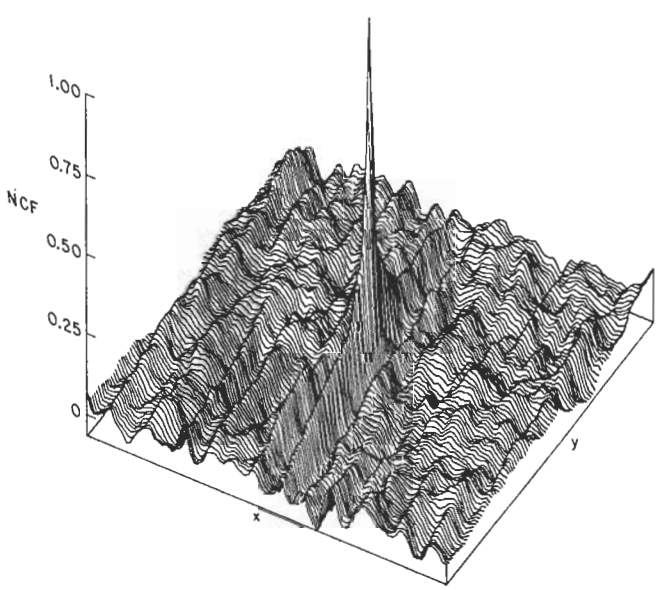

Fig. 7. The normalized covariance function of the sub-image with the main image of Figure 6. The NCF was calculated at every other grid point. A definite asymmetry is present with the peak being broader in the Y-direction than in the X-direction.

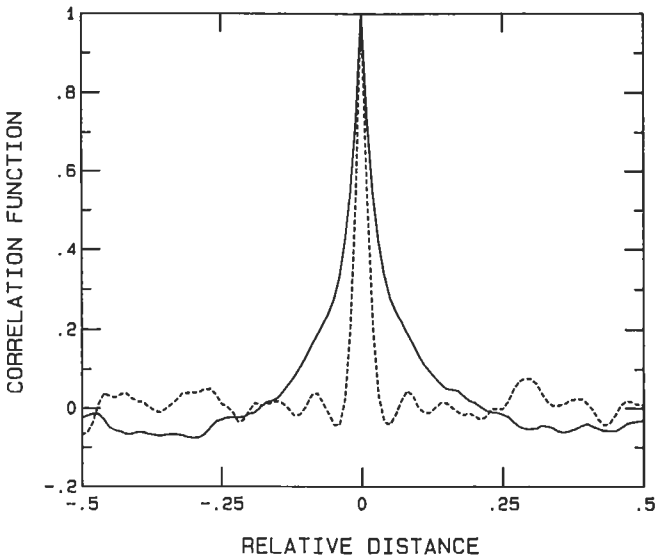

Fig. 8. One-dimensional cross-sections through the center of the two-dimensional NCF displayed in Figure 7. The solid line is parallel to the Y-axis and the dashed line is parallel to the X-axis. The correlation length is approximately 1.5 mm in Y and 0.5 mm in X.

There are many other applications for an inexpensive personal computer-based image-processing system. We are currently expanding our software package to include utilities to examine such topics as the size distribution of vapor inclusions in ice, rime-accretion rates and densities, and number concentrations in falling snow.

ACKNOWLEDGEMENTS

The authors should like to extend their appreciation to H. Greeley for his many helpful discussions and the generous use of his hardware. We should also like to thank R.T. Hall (Fig. 1) and Dr A.J. Gow (Fig. 5) for providing the photographs for this study.

REFERENCES

Arcone, S.A., Gow, A.J., *and* McGrew, S. 1986. Microwave dielectric, structural, and salinity properties of simulated sea ice. *IEEE Transactions on Geoscience and Remote Sensing*, **GE-24**(6), 832-39.

Carsey, F.D., *and* Zwally, H.J. 1986. Remote sensing as a research tool. *In* Untersteiner, N., *ed. The geophysics of sea ice*. New York, Plenum Press, 1021-98. (NATO ASI Ser. B, Physics, **146**.)

Greeley, H.P., Hirai, A., *and* Perovich, D.K. 1987. A review of the capabilities of a personal computer based image processing system. *CRREL Technical Note*.

Hall, R.T. 1984. *Data report: MIZEX 84 Polar Queen helicopter photography*. Seattle, WA, University of Washington. Applied Physics Laboratory. (Informal Document APL-UW 10-84.)

Langleben, M.P. 1972. The decay of an annual cover of sea ice. *Journal of Glaciology*, **11**(63), 337-44.

Matrox Electronics Systems Limited. 1986. *PIP user's manual*. Dorval, Canada, Matrox Electronic Systems Limited.

Maykut, G.A. 1982. Large-scale heat exchange and ice production in the central Arctic. *Journal of Geophysical Research*, **87**(C10), 7971-84.

Maykut, G.A., *and* Perovich, D.K. 1987. The role of shortwave radiation in the summer decay of a sea ice cover. *Journal of Geophysical Research*, **92**(C7), 7032-44.

Papoulis, A. 1965. *Probability, random variables and stochastic processes*. New York, McGraw-Hill.

Pavlidis, T. 1982. *Algorithms for graphics and image processing*. Rockville, MD, Computer Science Press.

Perovich, D.K. Unpublished. On the summer decay of a sea ice cover. (Ph.D dissertation, University of Washington, 1983.)

Stogryn, A. 1984. Correlation functions for random granular media in strong fluctuation theory. *IEEE Transactions on Geoscience and Remote Sensing*, **GE-22**(2), 150-54.

Tucker, W.B., *and* Hibler, W.D. 1987. *An evaluation of the polar ice prediction system. Final report*. Hanover, NH, U.S. Army Cold Regions Research and Engineering Laboratory.

Vallese, F., *and* Kong, J.A. 1981. Correlation function studies for snow and ice. *Journal of Applied Physics*, **52**(8), 4921-25.

MS. received 15 September 1987